



# Ex Vivo Human Tissue Functions as a Testing Platform for the Evaluation of a Nerve-Specific Fluorophore

Logan M. Bateman<sup>1,3</sup> · Samuel S. Streeter<sup>2,3</sup> · Kendra A. Hebert<sup>1</sup> · Dylan J. Parker<sup>3</sup> · Kaye Obando<sup>4</sup> · Kiara Sherlin Salas Moreno<sup>4</sup> · George J. Zanazzi<sup>3,6</sup> · Connor W. Barth<sup>4</sup> · Lei G. Wang<sup>4,5</sup> · Summer L. Gibbs<sup>4,5</sup> · Eric R. Henderson<sup>1,2,3</sup>

Received: 29 July 2024 / Revised: 2 October 2024 / Accepted: 13 November 2024 / Published online: 10 December 2024  
© The Author(s), under exclusive licence to World Molecular Imaging Society 2024

## Abstract

**Significance** Selecting a nerve-specific lead fluorescent agent for translation in fluorescence-guided surgery is time-consuming and expensive. Preclinical fluorescent agent studies rely primarily on animal models, which are a critical component of preclinical testing, but these models may not predict fluorophore performance in human tissues.

**Aim** The primary aim of this study was to evaluate and compare two preclinical models to test tissue-specific fluorophores based on discarded human tissues. The secondary aim was to use these models to determine the ability of a molecularly targeted fluorophore, LGW16-03, to label ex vivo human nerve tissues.

**Approach** Patients undergoing standard-of-care transtibial or transfemoral amputation were consented and randomized to topical or systemic administration of LGW16-03 following amputation. After probe administration, nerves and background tissues were surgically resected and imaged to determine nerve fluorescence signal-to-background tissue ratio (SBR) and signal-to-noise ratio (SNR) metrics. Analysis of variance (ANOVA) determined statistical differences in metric means between administration cohorts and background tissue groups. Receiver operating characteristic (ROC) curve-derived statistics quantified the discriminatory performance of LGW16-03 fluorescence for labeling nerve tissues.

**Results** Tissue samples from 18 patients were analyzed. Mean nerve-to-adipose SBR was greater than nerve-to-muscle SBR ( $p=0.001$ ), but mean nerve-to-adipose SNR was not statistically different from mean nerve-to-muscle SNR ( $p=0.069$ ). Neither SBR nor SNR means were statistically different between fluorophore administration cohorts ( $p \geq 0.448$ ). When administration cohorts were combined, nerve-to-adipose SBR was greater than nerve-to-muscle SBR (mean  $\pm$  standard deviation;  $4.2 \pm 2.9$  vs.  $1.8 \pm 1.9$ ;  $p < 0.001$ ), but SNRs for nerve-to-adipose and nerve-to-muscle were not significantly different ( $5.1 \pm 4.0$  vs.  $3.1 \pm 3.4$ ;  $p=0.055$ ). ROC curve-derived statistics to quantify LGW16-03 nerve labeling performance varied widely between patients, with sensitivities and specificities ranging from 0.2–99.9% and 0.4–100.0%.

**Conclusion** Systemic and topical administration of LGW16-03 yielded similar fluorescence labeling of nerve tissues. Both administration approaches provided nerve-specific contrast similar to that observed in preclinical animal models. Fluorescence contrast was generally higher for nerve-to-adipose versus nerve-to-muscle. Ex vivo human tissue models provide safe evaluation of fluorophores in the preclinical phase and can aid in the selection of lead agents prior to first-in-human trials.

**Keywords** Fluorescence-guided surgery · Lead agent selection · Nerve-specific fluorescence

✉ Eric R. Henderson  
Eric.R.Henderson@hitchcock.org

<sup>1</sup> Thayer School of Engineering, Dartmouth College, Hanover, NH 03755, USA

<sup>2</sup> Department of Orthopaedics, Dartmouth Health, Lebanon, NH 03756, USA

<sup>3</sup> Geisel School of Medicine, Dartmouth College, Hanover, NH 03755, USA

<sup>4</sup> Biomedical Engineering Department, Oregon Health and Science University, Portland, OR 97201, USA

<sup>5</sup> Knight Cancer Institute, Oregon Health and Science University, Portland, OR 97201, USA

<sup>6</sup> Department of Pathology and Laboratory Medicine, Dartmouth Health, Lebanon, NH 03756, USA

## Introduction

Fluorescence-guided surgery (FGS) is a rapidly growing field that uses fluorescent chemical compounds (fluorophores) to label specific tissues (*e.g.*, tumor, nerve) or physiological phenomena (*e.g.*, blood perfusion), thereby improving the surgeon's visualization of key features in the surgical field. Different mechanisms of labeling are used, namely non-targeted intravascular/intraluminal perfusion probes, molecularly targeted probes, and enzymatically or metabolically activated probes. One area of focus in the field of FGS is the development and evaluation of probes that specifically target nerves. This focus is motivated by the high prevalence of iatrogenic peripheral nerve injuries (PNIs) [1–6] and the potential of nerve-specific FGS to reduce the likelihood of intraoperative PNI [7–11].

Clinical translation of an FGS imaging agent requires United States Food and Drug Administration (FDA) approval. Currently, seven fluorophores (and fluorophore precursors) are approved by FDA for FGS: indocyanine green (ICG), methylene blue, fluorescein, 5-aminolevulinic acid, hexaminolevulinic acid hydrochloride (brand name Cysview, Photocure, Inc., Princeton, NJ; a precursor to 5-ALA), pafolacianine (known as OTL-38, brand name Cytalux, On Target Laboratories, LLC, West Lafayette, IN); and most recently, pegulicainine (brand name Lumisight, Lumicell, Newton, MA) [12–14]. Several other fluorescent agents are currently in late-stage clinical trials and demonstrate clinically advantageous performance [15–18]. Fluorescence imaging agents have no desired therapeutic effect, but therapeutic drugs provide a reasonable benchmark for the substantial cost and time required for securing FDA approval. The high cost of pivotal efficacy trials for new therapeutic agents (mean of \$19 million as of 2020) and long timeline for successful translation are known barriers to FDA approval, creating incentive to only select lead fluorescent agents with the strongest likelihood for success for evaluation in humans [13, 19].

FGS using a nerve-specific fluorophore has the potential to improve real-time identification and visualization of nerves in the surgical field, thereby reducing iatrogenic PNI and improving patient outcomes in terms of motor function and pain reduction [9, 20–23]. We have previously developed a library of synthetically engineered, oxazine-based, red- and near-infrared, nerve-specific fluorophores [9, 11]. LGW16-03 is a lead agent undergoing preclinical evaluation for intraoperative visualization of nerves to reduce iatrogenic PNI (peak excitation/emission of 626/655 nm when suspended in phosphate buffered saline) [16]. Animal models are critical for preclinical evaluation of fluorescent imaging agents. However, not all high performing agents in animal models will translate

in human trials [24, 25]. Understanding fluorophore performance in viable human tissue in the preclinical phase could improve the accuracy and safety of lead probe selection, thereby reducing the cost, time, and potential harm to patients in clinical trials [26].

A possible solution is to integrate *ex vivo* human tissues into preclinical testing. Testing with *ex vivo* human tissue is not novel in biomedical research [27, 28], and the approach has been most widely used in transplant surgery [29–33]. Freshly amputated human limbs represent an ideal environment for testing lead agents in human tissue without any risk associated with patients. Recently, a single amputated limb was perfused with LGW16-03 and imaged, demonstrating a proof-of-concept for fluorophore preclinical testing using *ex vivo* human tissue [26]. The primary goal of the present study was to extend our proof-of-concept results using a larger patient cohort. The secondary goal was to statistically compare nerve-specific fluorescent labeling when LGW16-03 was administered systemically using our established limb perfusion model versus a simplified topical administration protocol.

## Methods

### Study Enrollment

All aspects of this study were approved by the Dartmouth Health Institutional Review Board. The study enrolled patient receiving transtibial or transfemoral amputation for severe trauma, infection, or vascular insufficiency; oncological indications were also acceptable if the specimen did not need to be analyzed for margin status. Equal (1:1) proportions of patients with and without peripheral neuropathy were enrolled; neurological function was assessed by standard-of-care 5.07 Semmes–Weinstein monofilament testing [34]. All patients were randomized (1:1) to one of two study cohorts: systemic administration of LGW16-03 via vascular cannulization of the amputated limb or topical application of LGW16-03.

### Specimen Procurement

All amputation operations occurred in the main operating room at Dartmouth Hitchcock Medical Center (DHMC, Lebanon, New Hampshire). All specimens were then transferred to DHMC's Center for Surgical Innovation (CSI) for fluorophore administration and imaging.

### Topical Fluorophore Administration

For topical fluorophore administration, limbs were dissected to remove the tibial and/or peroneal nerves and adipose and

muscle samples adjacent to the nerves. Samples were submerged in a fluorophore bath consisting of 0.05 mg/mL LGW16-03 suspended in phosphate buffered saline (PBS). Each sample was bathed for five minutes followed by three 30-s washes in PBS prior to imaging.

### Systemic Fluorophore Administration

For systemic fluorophore administration, a perfused, amputated human limb model was used [26]. A dominant artery in the limb (*i.e.*, superficial femoral, anterior tibial, or posterior tibial artery, based upon the level of amputation, vessel diameter, and vessel patency) was identified, dissected, transected, and connected to a cardiopulmonary bypass machine (S3, Sorin Stockert, Breisgau, Germany) using a sized vascular cannula and a #0 silk suture. Limbs were perfused with sterile saline at 90–180 mL/min to maintain pressure within a physiological range (< 120 mmHg). A needle probe (Stryker, Kalamazoo, MI) verified in-line pressure throughout each perfusion experiment. Instead of venous cannulation for return, limbs drained by gravity, and the perfusate was collected in a reservoir and then recycled into the circuit. Within 10 min of establishing perfusion, a standard dose of LGW16-03 (1 mg/mL concentration suspended in PBS; 10 mL total) was administered intra-arterially. Fluorophore perfusion continued for 10 min, then the perfusate was swapped to plain saline for a 20-min washout. After the washout period, target nerve(s) (*i.e.*, common peroneal and/or tibial) and background tissues (*i.e.*, muscle, adipose) were resected for imaging. Specimens randomized to the systemic administration cohort with severe peripheral vascular disease that precluded vascular cannulization were excluded from further analysis.

### Fluorescence Imaging, Image Analysis, and Histopathology

Closed-field fluorescence imaging of tissue samples was performed with commercial systems (Odyssey CLx or Odyssey M using the 700 or 720 nm channel, respectively; LI-COR Biosciences, Lincoln, NE). All imaging data was collected using constant acquisition settings, except resolution settings which ranged from 10–100  $\mu\text{m}$ . To address inter-sample/inter-measurement variabilities, all nerve fluorescence measurements underwent intra-patient normalization to background tissues; all nerve fluorescence measurements were thus presented as signal-to-background ratio (SBR) and signal-to-noise ratio (SNR) metrics. All image analyses were performed using MATLAB (vR2022a, Mathworks, Natick, MA). Two-dimensional Gaussian filtering, implemented using the function `imgaussfilt` with a standard deviation of 10 pixels, reduced the resolution of the fluorescence images such that they exhibited macroscale, diffuse fluorescence

representative of what would be seen in the surgical field. Regions of interest (ROIs) were manually drawn around tissue samples, and descriptive pixel statistics (*i.e.*, mean, median, standard deviation) were extracted from each ROI and recorded. For every combination of nerve tissue ROI(s) and background tissue ROI(s) within a single patient, SBR and SNR were quantified to evaluate the ability of LGW16-03 to label nerve tissues. SBR and SNR were both calculated to demonstrate the variability in quantitative assessment between these metrics (Fig. 1) [35].

The experimental and image analysis workflow for the study is summarized in Fig. 1. Fluorophore administration cohorts are illustrated in Fig. 1a. The fluorescence metrics are defined in Fig. 1b, where  $\mu$  is the ROI pixel mean, and  $\sigma$  is the ROI pixel standard deviation. After imaging, limbs were taken to the Department of Pathology and Laboratory Medicine for standard-of-care processing. Permanent section histopathological staining with hematoxylin and eosin (H&E) confirmed tissue type.

### Statistical Analysis

All statistical analyses were implemented using MATLAB (vR2022a, MathWorks, Natick, MA). One-way and two-way analyses of variance (ANOVA) tested the hypothesis that SBR (or SNR) across groups (*i.e.*, nerve-to-adipose versus nerve-to-muscle metrics and systemic versus topical administration) were drawn from populations with the same mean SBR (or SNR). One-way ANOVA was implemented using the function `anova1` with default settings. Two-way ANOVA was implemented using the function `anovan` with the “interaction” argument to evaluate main effects of each grouping individually and the two-factor interaction.

A fluorescence SBR of  $\geq 1.5$  is considered useful for distinguishing features in open-field FGS [36]. As such, all SBR distributions—stratified by administration cohort and by background tissue—underwent an additional hypothesis test to evaluate the null hypothesis that each SBR distribution came from a population with mean equal to 1.5, against the alternative that the mean SBR was greater than 1.5 using a right-tailed *t*-test (`ttest` function).

Receiver operating characteristic (ROC) curve analysis determined the discriminatory performance of LGW16-03 fluorescence for labeling nerve tissues in each patient. Single-patient ROC curves enabled individual examination of the discriminatory performance of LGW16-03 fluorescence to label nerves versus background tissues. The Youden Index defined the optimal ROC cutoff point for determining sensitivity and specificity [37].

Linear regression using the function `fitlm` with default settings determined whether a statistical relationship was found between amputated limb neuropathy status and quantified SBR and SNR values. Results were reported as

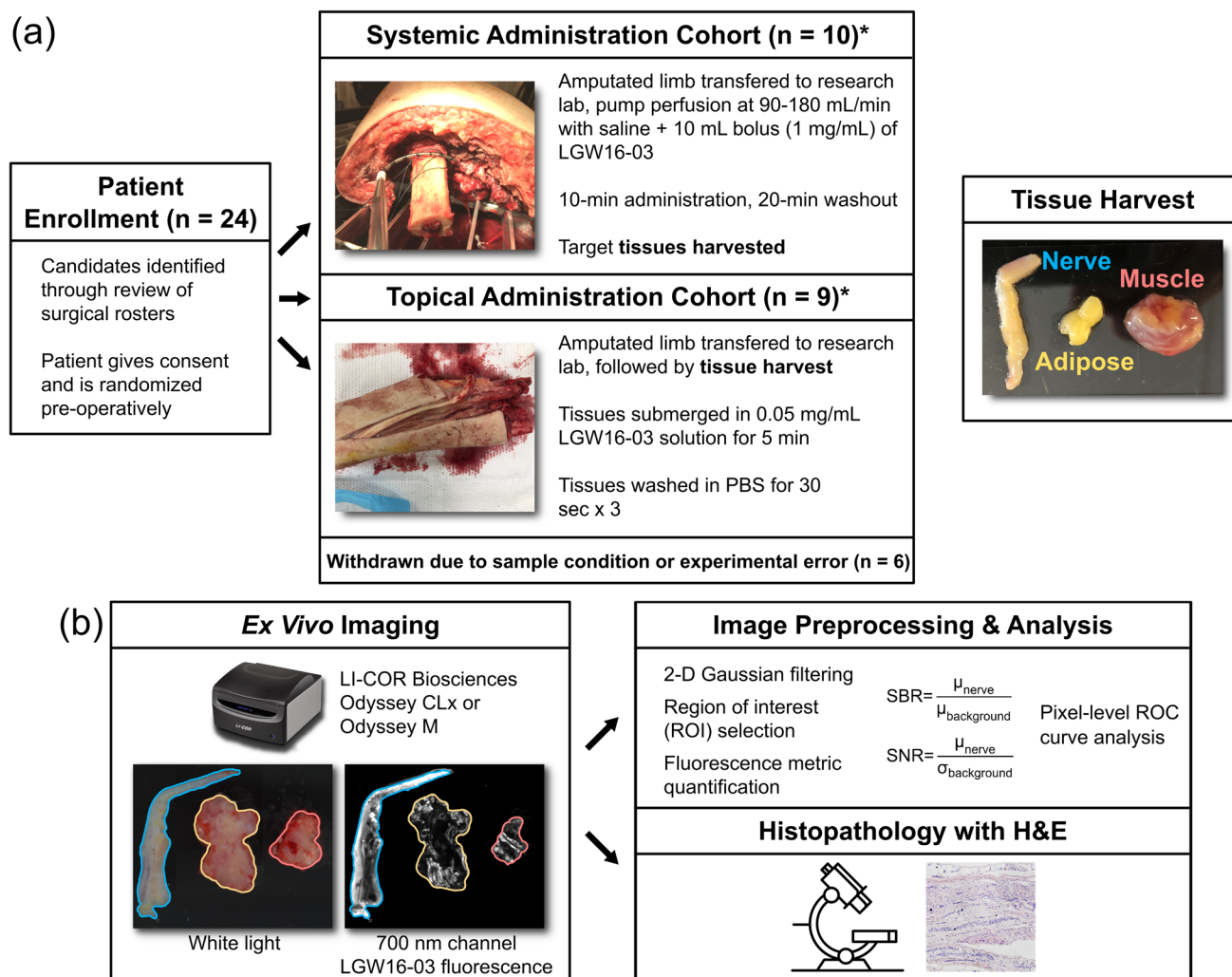


**Fig. 1** Experimental and analysis workflow for the study: **(a)** patient consent, enrollment, and randomization to either the systemic administration or topical administration of LGW16-03 cohorts. Fluorophore administration and target tissue harvesting (nerve [blue], adipose [yellow] and muscle [red]); **(b)** ex vivo fluorescence imaging followed by image preprocessing and metric quantification. Histopathological

tissue analysis using hematoxylin and eosin (H&E) stain confirmed tissue type. \*Tissues from one patient were analyzed in both administration cohorts. PBS = phosphate-buffered saline. SBR = signal-to-background ratio. SNR = signal-to-noise ratio. ROC = receiver operating characteristic

unstandardized coefficient estimates (B). For all statistical analyses, a p-value < 0.05 was considered statistically significant.

## Results

A total of 24 patients were enrolled. Tissue samples from a total of 18 patients (one amputated limb per patient) were analyzed. Six patients were withdrawn due to the inability to cannulate a dominant artery after amputation or due to technical errors during fluorophore administration. A total of 66 ex vivo tissue samples were fluorescently labeled and imaged, generating a total of 56 unique, patient-level

nerve-to-background tissue fluorescence measurements. All imaged tissues in the systemic and topical administration cohorts are shown in Supplemental Fig. 1 and 2, respectively. Table 1 summarizes the limbs and tissue samples analyzed. All raw ROI descriptive statistics (*i.e.*, mean, median, standard deviation) were also recorded (see systemic and topical administration cohort statistics in Supplemental Table 1 and 2, respectively). SBR and SNR results categorized by fluorophore administration cohort and by background tissue type are plotted in Fig. 2 (and are tabulated in Supplemental Table 3 and 4).

Nerve-to-adipose SBR for topical administration of fluorophore was (mean ± standard deviation)  $4.6 \pm 2.5$ ; for systemic fluorophore administration, nerve-to-adipose SBR was

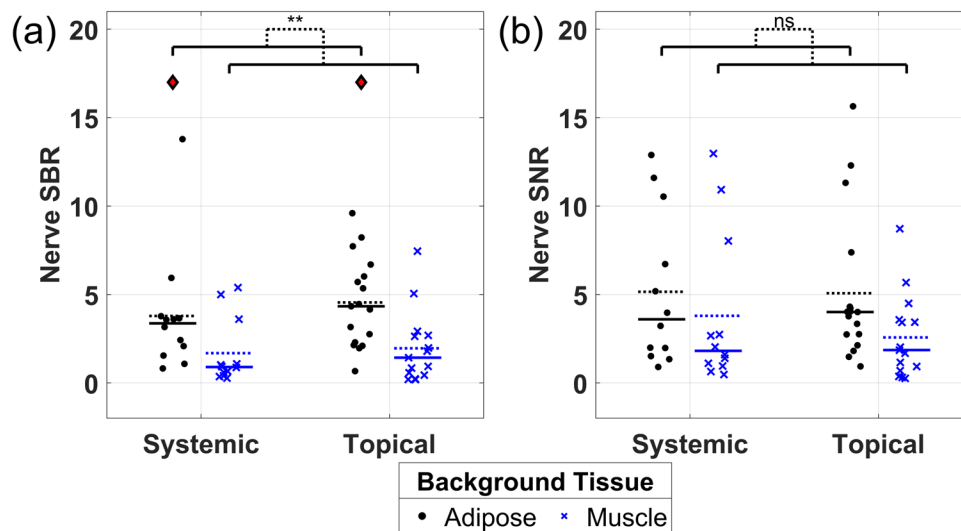


**Fig. 2** Fluorescence tissue signal (a) signal-to-background ratio (SBR) and (b) signal-to-noise ratio (SNR) for nerve-to-adipose (black) and nerve-to-muscle (blue). Legend in (b) applies to both subplots. Dashed/solid horizontal lines = means/medians. Systemic = systemic administration of LGW16-03 cohort. Topical = topical admin-

istration of LGW16-03 cohort. Two-way ANOVA statistical test results: no annotation = not significant; \* =  $p < 0.05$ ; \*\* =  $p < 0.01$ ; \*\*\* =  $p < 0.001$ . Red diamond = cohort measurements from population with mean SBR  $> 1.5$  ( $p < 0.05$ )

**Table 1** Patient limb and tissue sample details

Variable	Count (%)
Enrollment and analysis, no. of patients/limbs	18
Limb neuropathy status, no. of limbs	
Negative	7 (39)
Positive	10 (56)
Unknown	1 (6)
Fluorophore administration cohort, no. of limbs	
Systemic	10 (56)*
Topical	9 (50)*
Tissues samples, no. of samples in systemic/topical cohorts	
Adipose	10/9
Muscle	10/8
Nerve	12/17
Total no. of samples in both cohorts	66
Nerve-to-background measurements, no. in systemic/topical cohorts	
Nerve-to-adipose	12/17
Nerve-to-muscle	12/15
Total no. of nerve-to-background measurements in both cohorts	56

\*One patient limb underwent analysis in both systemic and topical cohorts; for this case, representative tissues were first resected for topical administration of LGW16-03, then the limb underwent perfusion, systemic administration of LGW16-03, and tissue resection as described

$3.8 \pm 3.5$ . Nerve-to-muscle SBR for topical administration was  $2.0 \pm 2.0$ ; for systemic administration, nerve-to-muscle SBR was  $1.7 \pm 1.9$ . Nerve-to-adipose SNR for topical administration of fluorophore was  $5.1 \pm 4.2$ ; for systemic fluorophore administration, nerve-to-adipose SNR was  $5.2 \pm 4.3$ . Nerve-to-muscle SNR for topical administration

was  $2.6 \pm 2.4$ ; for systemic administration, nerve-to-muscle SNR was  $3.8 \pm 4.3$ . These data were analyzed using two-way ANOVA. Nerve-to-background tissue SBRs exhibited no significant differences between fluorophore administration cohorts ( $p = 0.448$ ). Similarly, SNRs exhibited no significant differences between administration cohorts ( $p = 0.532$ ).

Nerve-to-adipose SBR was significantly greater than nerve-to-muscle SBR ( $p=0.001$ ). However, nerve-to-adipose SNR was not significantly different than nerve-to-muscle SNR ( $p=0.069$ ). Nerve-to-adipose SBR distribution means for both administration cohorts were statistically greater than 1.5 based on a right-tailed t-test ( $p\leq 0.021$ ; noted by red diamond in Fig. 2a), but no nerve-to-muscle SBR distribution means were statistically greater than 1.5 ( $p\geq 0.198$ ). Complete two-way ANOVA results are tabulated in Supplemental Table 5 and 6.

Figure 3 shows the same data as Fig. 2 reorganized such that the two fluorophore administration cohorts were combined. These data were analyzed using one-way ANOVA. Combined nerve-to-adipose SBR was statistically greater than combined nerve-to-muscle SBR ( $4.2\pm 2.9$  vs.  $1.8\pm 1.9$ ;  $p<0.001$ ). However, no significant difference in SNR was found (nerve-to-adipose SNR versus -to-muscle SNR of  $5.1\pm 4.0$  vs.  $3.1\pm 3.4$ ;  $p=0.055$ ). The combined nerve-to-adipose SBR distribution mean was statistically greater than 1.5 based on a right-tailed t-test ( $4.2\pm 2.9$ ;  $p<0.001$ ; noted by red diamond in Fig. 3a), but the combined nerve-to-muscle SBR distribution mean was not statistically greater than 1.5 ( $1.8\pm 1.9$ ;  $p=0.186$ ). Complete one-way ANOVA results are tabulated in Supplemental Table 7 and 8.

The neuropathy status of limbs had a statistically significant impact on SBR values within the topically administered cohort based on linear regression, indicating a substantial reduction in SBR with neuropathy ( $B=-2.62$ ;  $p=0.001$ ). However, neuropathy status had no significant relationship with SBR values in the systemically administered cohort or any SNR values. Complete regression results are tabulated in Supplemental Tables 9–12, broken down by administration cohort and metric (SBR/SNR).

ROC curves and associated performance statistics (i.e., sensitivity, specificity, accuracy, and area under the curve) for discriminating nerve pixels from background tissue pixels are shown in Supplemental Fig. 3 and 4 for the systemic

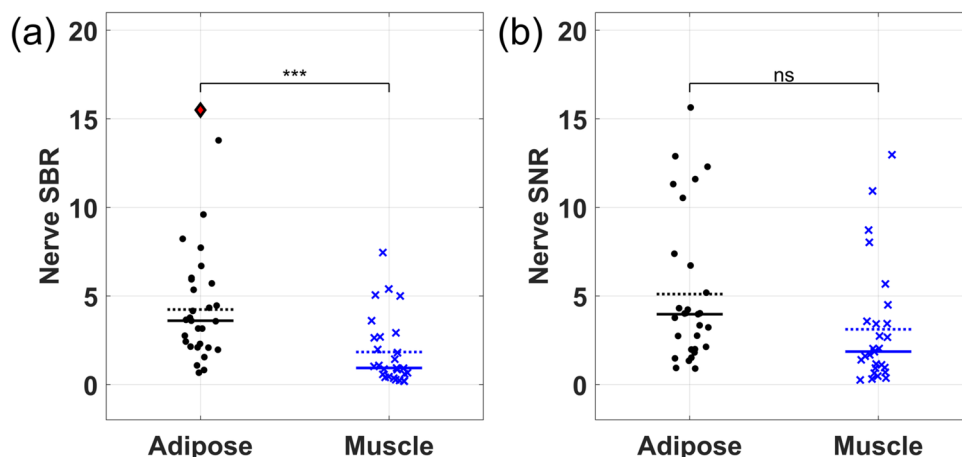
and topical administration cohorts, respectively. Corroborating results in Figs. 2 and 3, showed some patients exhibited high discriminatory power for identifying nerve tissue (e.g., Patient 15 in the systemic cohort achieved statistics all  $\geq 94.4\%$ ; Patient 10 in the topical cohort achieved statistics all  $\geq 85.5\%$ ). However, other patients exhibited relatively poor labeling of nerves (e.g., Patient 2 in the systemic cohort achieved sensitivity, specificity, accuracy, and area under the curve of 0.5%, 99.7%, 48.7%, and 35.5%, respectively).

## Discussion

This study is an extension of a prior, proof-of-concept study to evaluate preclinical testing of a nerve-specific fluorophore in an amputated human limb [26]. Results herein included tissues from 18 patients' lower limbs, 10 of which were used in the limb perfusion model for systemic administration of LGW16-03 (Fig. 1, Table 1). No statistically significant difference in nerve-specific SBR or SNR was found between systemic and topical administration of LGW16-03. Fluorescence contrast was generally higher for nerve-to-adipose versus nerve-to-muscle; nerve-to-adipose SBRs for both administration cohorts exhibited sample means statistically  $> 1.5$ , suggesting a useful level of contrast for FGS [36]. These results corroborate oxazine-based, nerve-specific fluorescence SBRs reported previously in preclinical murine models (SBRs up to  $\sim 5$  for topical administration and up to  $\sim 4$  for systemic administration) [9, 11]. Although mean nerve-to-muscle SBRs for both administration cohorts in the present study were  $> 1.5$  (systemic and topical cohorts yielded SBRs of 1.7 and 2.0, respectively), measurement variances were significant in both groups such that mean nerve-to-muscle SBRs were not  $> 1.5$  with statistical significance.

Neuropathy status did not have a broad impact on nerve SBR or SNR measurements, but within the topically administered cohort, nerve SBRs were significantly related to

**Fig. 3** Fluorescence tissue signal (a) signal-to-background ratio (SBR) and (b) signal-to-noise ratio (SNR) for nerve-to-adipose (black) and nerve-to-muscle (blue) with systemic and topical administration cohorts combined. Dashed/solid horizontal lines = means/medians. CNR = contrast-to-noise ratio. One-way ANOVA statistical test results: ns = not significant; \* =  $p<0.05$ ; \*\* =  $p<0.01$ ; \*\*\* =  $p<0.001$ . Red diamond = cohort measurements from population with mean SBR  $> 1.5$



neuropathy status. Because topical administration of fluorophore is independent of tissue perfusion, we hypothesize that this trend is due to a diminished expression level of the LGW16-03 molecular target in neuropathic nerves.

The high variances observed in LGW16-03 fluorescent measurements (Figs. 2 and 3) and corresponding ROC curve-derived statistics for labeling nerve tissues (Supplemental Fig. 3 and 4) may be due to experimental limitations. Systemic administration protocol involved a 10-min LGW16-03 perfusion followed by 20 min of saline wash-out; this administration-to-imaging time is relatively short for optimal nerve-agent binding based on preclinical studies of LGW16-03. Limb perfusion experiments were time-limited by the known ischemic time of amputated limbs [32]. Additionally, measurement variances could be the result of physiological variabilities in the amputated limbs themselves. Although an enrollment exclusion criterion was severe peripheral vascular disease, and neuropathy status was recorded for each enrollment, thorough physiological and histological characterization of amputated limbs imaged in this study was not performed and will be the subject of future work.

Patients requiring amputation due to peripheral artery disease (PAD) often have had prior surgical salvage attempts [38, 39] and/or poorly controlled diabetes associated with infection [40]. Thus, these limbs often contain heavily calcified arteries and muscle that has undergone chronic ischemia due to PAD. Muscle affected by chronic ischemia has reduced fiber density, fiber size, and increased fatty infiltrate [41–43]. Reduced muscle fiber density could create an environment amenable to passive diffusion of LGW16-03 into muscular compartments where it was retained, leading to atypically high fluorescence in some muscle samples (*e.g.*, Supplemental Fig. 1a and f, and Supplemental Fig. 2a, h, i). This enhanced permeability and retention effect is supported by studies that induced PAD in rodent hindlimbs and demonstrated increased accumulation of nanoparticles in muscle tissue [44]. In addition, angiogenic factors are upregulated in chronically ischemic tissues, which may mobilize endothelial cells to form leaky vasculature like that seen in tumors [45].

Extended periods of normothermic machine perfusion using standards for vascular composite allografts (VCA) could improve the quality and viability of *ex vivo* human tissue models [31–33]. The use of an oxygen carrying blood product, electrolytes, and other nutrients (*e.g.*, glucose, insulin) in the perfusate could extend the *ex vivo* timeframe of tissue viability. Steroids within the perfusate could reduce the amount of vascular leakage as well (*e.g.*, methylprednisolone) [32]. Indeed, best available practice VCA protocols can support limb viability for 40 h and beyond. Limbs in these experiments experienced a normalization period during which limb pressure, pH, and blood laboratory values

stabilized over a six-hour period, allowing for increased perfusion time and increased tissue viability [33]. The evolving field of VCA is not widely adopted. These protocols may, however, vastly improve limb viability and allow for more accurate study of fluorophores using amputated limbs. The limbs used within these VCA studies were obtained through academic medical center-affiliated limb donation programs. These programs, combined with established global cadaver donation programs [46], set a precedent for the respectful use of *ex vivo* human tissues in medicine—training and research—more broadly, including preclinical evaluation of FGS imaging agents.

## Conclusion

Nerve-specific FGS has the potential to improve real-time, wide field-of-view visualization of nerves in the surgical field, reducing the prevalence of iatrogenic PNI and improving patient outcomes in terms of motor function and pain reduction. *Ex vivo* human tissue models provide a safe and biomarker-relevant platform for the evaluation of fluorophores in the preclinical phase with zero additional risk to patients and can aid in the selection of lead agents prior to first-in-human trials.

**Supplementary Information** The online version contains supplementary material available at <https://doi.org/10.1007/s11307-024-01968-0>.

**Acknowledgements** This work was funded by NIH Grants 1K23EB026507 and 1R01NS116994-01A1.

**Data Availability** Raw imaging data is available upon reasonable request made to corresponding author.

## References

1. Robinson LR (2000) Traumatic injury to peripheral nerves. *Muscle Nerve* 23(6):863–873. [https://doi.org/10.1002/\(SICI\)1097-4598\(200006\)23:6](https://doi.org/10.1002/(SICI)1097-4598(200006)23:6)
2. Kretschmer T, Antoniadis G, Braun V, Rath SA, Richter HP (2001) Evaluation of iatrogenic lesions in 722 surgically treated cases of peripheral nerve trauma. *J Neurosurg* 94(6):905–912. <https://doi.org/10.3171/jns.2001.94.6.0905>
3. Burke S, Shorten GD (2009) When pain after surgery doesn't go away.... *Biochem Soc Trans* 37(1):318–322. <https://doi.org/10.1042/BST0370318>
4. Haanpää M, Attal N, Backonja M, Baron R, Bennett M, Bouhassira D, Cruccu G, Hansson P, Haythornthwaite JA, Iannetti GD, Jensen TS, Kauppila T, Nurmikko TJ, Rice ASC, Rowbotham M, Serra J, Sommer C, Smith BH, Treede R-D (2011) NeuPSIG guidelines on neuropathic pain assessment. *Pain* 152(1):14–27. <https://doi.org/10.1016/j.pain.2010.07.031>
5. Grinsell D, Keating CP (2014) Peripheral nerve reconstruction after injury: a review of clinical and experimental therapies. *BioMed Res* 2014:698256. <https://doi.org/10.1155/2014/698256>

6. Osborne NR, Anastakis DJ, Davis KD (2018Apr 1) Peripheral nerve injuries, pain, and neuroplasticity. *J Hand Ther* 31(2):184–194. <https://doi.org/10.1016/j.jht.2018.01.011>
7. Barth CW, Gibbs SL (2017) Direct administration of nerve-specific contrast to improve nerve sparing radical prostatectomy. *Theranostics* 7(3):573–593. <https://doi.org/10.7150/thno.17433>
8. Walsh EM, Cole D, Tipirneni KE, Bland KI, Udayakumar N, Kastent BB, Bevans SL, McGrew BM, Kain JJ, Nguyen QT, Rosenthal EL, Warram JM (2019) Fluorescence imaging of nerves during surgery. *Ann Surg* 270(1):69–76. <https://doi.org/10.1097/SLA.0000000000003130>
9. Wang LG, Barth CW, Kitts CH, Mebrat MD, Montañó AR, House BJ, McCoy ME, Antaris AL, Galvis SN, McDowall I, Sorger JM, Gibbs SL (2020) Near-infrared nerve-binding fluorophores for buried nerve tissue imaging. *Sci Transl Med* 12(542):eaay0712. <https://doi.org/10.1126/scitranslmed.aay0712>
10. Barth CW, Shah VM, Wang LG, Masillati AM, Al-Fatease A, Husain Rizvi SZ, Antaris AL, Sorger J, Rao DA, Alani AWG, Gibbs SL (2022May) A clinically relevant formulation for direct administration of nerve specific fluorophores to mitigate iatrogenic nerve injury. *Biomaterials* 1(284):121490. <https://doi.org/10.1016/j.biomaterials.2022.121490>
11. Wang LG, Montañó AR, Masillati AM, Jones JA, Barth CW, Combs JR, Kumarapeli SU, Shams NA, van den Berg NS, Antaris AL, Galvis SN, McDowall I, Rizvi SZH, Alani AWG, Sorger JM, Gibbs SL (2024) Nerve Visualization using Phenoxazine-Based Near-Infrared Fluorophores to Guide Prostatectomy. *Adv Mater* 36(16):2304724. <https://doi.org/10.1002/adma.202304724>
12. Lotan Y, Bivalacqua TJ, Downs T, Huang W, Jones J, Kamat AM, Konety B, Malmström P-U, McKiernan J, O'Donnell M, Patel S, Pohar K, Resnick M, Sankin A, Smith A, Steinberg G, Trabulsi E, Woods M, Daneshmand S (2019) Blue light flexible cystoscopy with hexaminolevulinate in non-muscle-invasive bladder cancer: review of the clinical evidence and consensus statement on optimal use in the USA - update 2018. *Nat Rev Urol* 16(6):377–386. <https://doi.org/10.1038/s41585-019-0184-4>
13. Pogue BW, Rosenthal EL (2021) Review of successful pathways for regulatory approvals in open-field fluorescence-guided surgery. *J Biomed Opt* 26(3):030901. <https://doi.org/10.1117/1.JBO.26.3.030901>
14. Van Keulen S, Hom M, White H, Rosenthal EL, Baik FM (2023) The evolution of fluorescence-guided surgery. *Mol Imaging Biol* 25(1):36–45. <https://doi.org/10.1007/s11307-022-01772-8>
15. Crawford KL, Pacheco FV, Lee Y-J, Hom M, Rosenthal EL, Nguyen QT, Orosco RK (2022) A scoping review of ongoing fluorescence-guided surgery clinical trials in otolaryngology. *Laryngoscope* 132(1):36–44. <https://doi.org/10.1002/lary.29891>
16. Bou-Samra P, Muhammad N, Chang A, Karsalia R, Azari F, Kennedy G, Stummer W, Tanyi J, Martin L, Vahrmeijer A, Smith B, Rosenthal E, Wagner P, Rice D, Lee A, Abdelhafeez H, Malek MM, Kohanbash G, Edwards WB, Henderson E, Skjøth-Rasmussen J, Orosco R, Gibbs S, Farnam RW, Shankar L, Sumer B, Kumar ATN, Marcu L, Li L, Greuv V, Delikatny EJ, Lee JYK, Singhal S (2023) Intraoperative molecular imaging: 3rd biennial clinical trials update. *J Biomed Opt* 28(5):050901. <https://doi.org/10.1117/1.JBO.28.5.050901>
17. Miampamba M, Liu J, Harootunian A, Gale AJ, Baird S, Chen SL, Nguyen QT, Tsien RY, González JE (2017) Sensitive in vivo visualization of breast cancer using ratiometric protease-activatable fluorescent imaging agent, AVB-620. *Theranostics* 7(13):3369–3386. <https://doi.org/10.7150/thno.20678>
18. Yamada M, Miller DM, Lowe M, Rowe C, Wood D, Soyer HP, Byrnes-Blake K, Parrish-Novak J, Ishak L, Olson JM, Brandt G, Griffin P, Spelman L, Prow TW (2021) A first-in-human study of BLZ-100 (tozuleristide) demonstrates tolerability and safety in skin cancer patients. *Contemp Clin Trials Commun* 23:100830. <https://doi.org/10.1016/j.conctc.2021.100830>
19. Moore TJ, Zhang H, Anderson G, Alexander GC (2018) Estimated costs of pivotal trials for novel therapeutic agents approved by the US Food and Drug Administration, 2015–2016. *JAMA Intern Med* 178(11):1451–1457. <https://doi.org/10.1001/jamainternmed.2018.3931>
20. Wu C, Wei J, Tian D, Feng Y, Miller RH, Wang Y (2008) Molecular probes for imaging myelinated white matter in CNS. *J Med Chem* 51(21):6682–6688. <https://doi.org/10.1021/jm8003637>
21. Wang C, Popescu DC, Wu C, Zhu J, Macklin W, Wang Y (2010) In situ fluorescence imaging of myelination. *J Histochem Cytochem* 7:611–621. <https://doi.org/10.1369/jhc.2010.954842>
22. Cotero VE, Siclován T, Zhang R, Carter RL, Bajaj A, LaPlante NE, Kim E, Gray D, Staudinger VP, Yazdanfar S, Tan Hehir CA (2012) Intraoperative fluorescence imaging of peripheral and central nerves through a myelin-selective contrast agent. *Mol Imaging Biol* 14(6):708–717. <https://doi.org/10.1007/s11307-012-0555-1>
23. Hingorani DV, Whitney MA, Friedman B, Kwon J-K, Crisp JL, Xiong Q, Gross L, Kane CJ, Tsien RY, Nguyen QT (2018) Nerve-targeted probes for fluorescence-guided intraoperative imaging. *Theranostics* 8(15):4226–4237. PMID: PMC6096382. <https://doi.org/10.7150/thno.23084>
24. Barré-Sinoussi F, Montagutelli X (2015) Animal models are essential to biological research: issues and perspectives. *Future Sci OA* 1(4):FSO63. <https://doi.org/10.4155/fso.15.63>
25. Ruan Y, Robinson NB, Khan FM, Hameed I, Rahouma M, Naik A, Oakley CT, Rong L, Girardi LN, Gaudino M (2020) The translation of surgical animal models to human clinical research: A cross-sectional study. *Int J Surg* 77:25–29. <https://doi.org/10.1016/j.ijsu.2020.03.023>
26. Bateman LM, Hebert KA, Nunziata JA, Streeter SS, Barth CW, Wang LG, Gibbs SL, Henderson ER (2023) Preclinical evaluation of molecularly targeted fluorescent probes in perfused amputated human limbs. *J Biomed Opt* 28(8):082802. <https://doi.org/10.1117/1.JBO.28.8.082802>
27. Corzo-León DE, Munro CA, MacCallum DM (2019) An ex vivo human skin model to study superficial fungal infections. *Front Microbiol* 10. <https://doi.org/10.3389/fmicb.2019.01117>
28. Garcia-Garcia FC, Candarlioglu PL, Porter JD, Davies DE, Swindle EJ, Morgan H (2022Dec) Microfluidic technologies for ex vivo tissue biopsies: A review. *Organs-on-a-Chip* 1(4):100020. <https://doi.org/10.1016/j.ooc.2022.100020>
29. Cypel M, Yeung JC, Liu M, Anraku M, Chen F, Karolak W, Sato M, Laratta J, Azad S, Madonik M, Chow C-W, Chaparro C, Hutcheon M, Singer LG, Slutsky AS, Yasufuku K, de Perrot M, Pierre AF, Waddell TK, Keshavjee S (2011) Normothermic Ex Vivo Lung Perfusion in Clinical Lung Transplantation. *N Engl J Med* 364(15):1431–1440. <https://doi.org/10.1056/NEJMoa1014597>
30. Lam VWT, Laurence JM, Richardson AJ, Pleass HCC, Allen RDM (2013) Hypothermic machine perfusion in deceased donor kidney transplantation: a systematic review. *J Surg Res* 180(1):176–182. <https://doi.org/10.1016/j.jss.2012.10.055>
31. Elliott RM, Tintle SM, Levin LS (2014) Upper extremity transplantation: current concepts and challenges in an emerging field. *Curr Rev Musculoskelet Med* 7(1):83–88. <https://doi.org/10.1007/s12178-013-9191-x>
32. Werner NL, Alghanem F, Rakestraw SL, Sarver DC, Nicely B, Pietroski RE, Lange P, Rudich SM, Mendias CL, Rojas-Pena A, Magee JC, Bartlett RH, Ozer K (2017) Ex situ perfusion of human limb allografts for 24 hours. *Transplantation*. 101(3). Available from: [https://journals.lww.com/transplantjournal/Fulltext/2017/03000/Ex\\_Situ\\_Perfusion\\_of\\_Human\\_Limb\\_Allografts\\_for\\_24.34.aspx](https://journals.lww.com/transplantjournal/Fulltext/2017/03000/Ex_Situ_Perfusion_of_Human_Limb_Allografts_for_24.34.aspx)

33. Rezaei M, Ordenana C, Figueroa BA, Said SA, Fahradyan V, Dalla Pozza E, Orfahli LM, Annunziata MJ, Rohde E, Madajka M, Papay F, Rampazzo A, Bassiri Gharb B (2022) Ex vivo normothermic perfusion of human upper limbs. *Transplantation* 106(8):1638–1646. <https://doi.org/10.1097/TP.0000000000004045>
34. Perkins BA, Olaleye D, Zinman B, Bril V (2001) Simple screening tests for peripheral neuropathy in the diabetes clinic. *Diabetes Care* 24(2):250–256. <https://doi.org/10.2337/diacare.24.2.250>
35. LaRochelle EPM, Streeter SS, Littler EA, Ruiz AJ (2023Feb 1) 3D-Printed Tumor Phantoms for Assessment of In Vivo Fluorescence Imaging Analysis Methods. *Mol Imag Biol* 25(1):212–220. <https://doi.org/10.1007/s11307-022-01783-5>
36. Azargoshasb S, Boekestijn I, Roestenberg M, KleinJan GH, van der Hage JA, van der Poel HG, Rietbergen DDD, van Oosterom MN, van Leeuwen FWB (2023) Quantifying the impact of signal-to-background ratios on surgical discrimination of fluorescent lesions. *Mol Imaging Biol* 25(1):180–189. <https://doi.org/10.1007/s11307-022-01736-y>
37. Youden WJ (1950) Index for rating diagnostic tests. *Cancer* 3(1):32–35. [https://doi.org/10.1002/1097-0142\(1950\)3:1<32::aid-cnrcr2820030106>3.0.co;2-3](https://doi.org/10.1002/1097-0142(1950)3:1<32::aid-cnrcr2820030106>3.0.co;2-3)
38. Swaminathan A, Vemulapalli S, Patel MR, Jones WS (2014) Lower extremity amputation in peripheral artery disease: improving patient outcomes. *Vasc Health Risk Manag* 10:417–424. <https://doi.org/10.2147/VHRM.S50588>
39. Molina CS, Faulk J (2023) Lower Extremity Amputation. *StatPearls*. Treasure Island, FL: StatPearls Publishing
40. Pickwell K, Siersma V, Kars M, Apelqvist J, Bakker K, Edmonds M, Holstein P, Jirkovská A, Jude E, Mauricio D, Piaggese A, Ragnarson Tennvall G, Reike H, Spraul M, Uccioli L, Urbancic V, van Acker K, van Baal J, Schaper N (2015) Predictors of lower-extremity amputation in patients with an infected diabetic foot ulcer. *Diabetes Care* 38(5):852–857. <https://doi.org/10.2337/dc14-1598>
41. Regensteiner JG, Wolfel EE, Brass EP, Carry MR, Ringel SP, Hargarten ME, Stamm ER, Hiatt WR (1993) Chronic changes in skeletal muscle histology and function in peripheral arterial disease. *Circulation* 87(2):413–421. <https://doi.org/10.1161/01.cir.87.2.413>
42. Carmo-Araújo EM, Dal-Pai-Silva M, Dal-Pai V, Cecchini R, Anjos Ferreira AL (2007) Ischaemia and reperfusion effects on skeletal muscle tissue: morphological and histochemical studies. *Int J Exp Pathol* 88(3):147–154. <https://doi.org/10.1111/j.1365-2613.2007.00526.x>
43. McDermott MM, Ferrucci L, Gonzalez-Freire M, Kosmac K, Leeuwenburgh C, Peterson CA, Saini S, Sufit R (2020) Skeletal muscle pathology in peripheral artery disease: a brief review. *Arterioscler Thromb Vasc Biol* 40(11):2577–2585. <https://doi.org/10.1161/ATVBAHA.120.313831>
44. England CG, Im H-J, Feng L, Chen F, Graves SA, Hernandez R, Orbay H, Xu C, Cho SY, Nickles RJ, Liu Z, Lee DS, Cai W (2016) Re-assessing the enhanced permeability and retention effect in peripheral arterial disease using radiolabeled long circulating nanoparticles. *Biomater* 100:101–109. <https://doi.org/10.1016/j.biomaterials.2016.05.018>
45. Wahlberg E (2003) Angiogenesis and arteriogenesis in limb ischemia. *J Vasc Surg* 38(1):198–203. [https://doi.org/10.1016/s0741-5214\(03\)00151-4](https://doi.org/10.1016/s0741-5214(03)00151-4)
46. Porzionato A, Macchi V, Stecco C, Mazzi A, Rambaldo A, Sarasin G, Parenti A, Scipioni A, De Caro R (2012) Quality management of body donation program at the University of Padova. *Anat Sci Ed* 5(5):264–272. <https://doi.org/10.1002/ase.1285>

**Publisher's Note** Springer Nature remains neutral with regard to jurisdictional claims in published maps and institutional affiliations.

Springer Nature or its licensor (e.g. a society or other partner) holds exclusive rights to this article under a publishing agreement with the author(s) or other rightsholder(s); author self-archiving of the accepted manuscript version of this article is solely governed by the terms of such publishing agreement and applicable law.